Research Report

2001-06

Low Noise and Smooth Torque Permanent Magnet Propulsion Motors: Comparison of Non-slotted and Slotted Radial and Axial Flux Topologies

S. Huang*, M. Aydin, T.A. Lipo

*Department of Automation
Shanghai University
149 Yan-Chang Road
Shanghai, 200072, P.R. China

Wisconsin Power Electronic
Research Center
University of Wisconsin - Madison
Madison, WI 53706

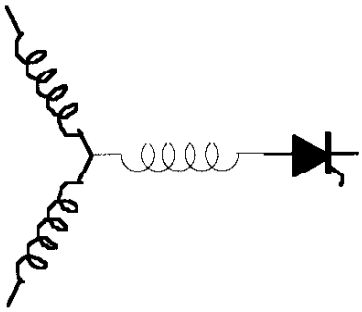

Wisconsin
Electric
Machines &
Power
Electronics
Consortium

University of Wisconsin-Madison
College of Engineering
Wisconsin Power Electronics Research Center
2559D Engineering Hall
1415 Engineering Drive
Madison WI 53706-1691

International Aegean Conference on Electrical Machines and Power Electronics, 2001

Low Noise and Smooth Torque Permanent Magnet Propulsion Motors: Comparison of Non-slotted and Slotted Radial and Axial Flux Topologies

Surong Huang**

Metin Aydin*
Student Member

Thomas A. Lipo*
Fellow, IEEE

**Department of Automation
Shanghai University
149 Yan-Chang Road
Shanghai, 200072, P.R. China

*Department of Electrical and Computer Engineering
University of Wisconsin-Madison
1415 Engineering Drive
Madison, WI 53706-1691, U.S.A

Email: aydin@cae.wisc.edu Tel: +1 (608)-265 38 15 Fax: +1 (608)-262 55 59

Abstract

In this paper, torque ripple factor (TRF) is introduced to analyze pulsating torque component of surface mounted permanent magnet (PM) machines. Based on the torque and sizing analysis, optimum design can be achieved for minimum ripple torque and maximum torque density. PM pole arc ratio and magnet skew angle are chosen both to minimize the ripple torque and to optimize the machine performance. The resultant plots are shown using 2D and 3D plots. Moreover, 2D and 3D Finite Element Analysis (FEA) of both axial flux and radial flux surface mounted motor structures (TORUS, AFIR and RFSM) are investigated for pulsating torques, ripple torques and cogging torques. Results obtained from both sizing equations, TRF analysis and results obtained from 2D/3D FEA were completed and are illustrated in the paper.

1. Introduction

The search for a low noise and smooth torque motor has been sought for decades without a completely satisfactory solution. This difficulty has resulted from the emphasis that has been placed on the design of squirrel cage induction machines for such purposes. Unfortunately, induction machines, by their nature, have large number of inherent noise producing mechanisms due to the effects of slotting the stator and rotor. Consequently, these mechanisms cause noise producing permeance harmonics and necessitate placing windings in discrete slots resulting in noise producing MMF harmonics. The interaction between these two harmonic components produces additional force and torque producing harmonics and further complicates the issue. Finally, inverter-driven machines result in time harmonics impressed on the windings of the stator that can interact with the space harmonics to produce an additional measure of torque pulsations and audible noise.

One alternative to radial flux squirrel cage induction motors is a radial flux permanent magnet (PM) motor. Permanent magnet motors offer many advantageous features. They are usually more efficient because field excitation losses are eliminated. Rotor losses are reduced in PM machines compared to induction machines because they lack the rotor windings and field excitation in the rotor. Moreover, PM motors have small magnetic thickness which results in the fact that PM machines can be smaller than the other machines in terms of size. Therefore, the total mass of the machine goes down. However, these machines still contain noise and vibration sources. They also have the ability of developing magnetic stress in the machine airgap and various parts of the motor without use of stator current. One other alternative to radial flux machines are disc type axial flux PM machines [2-4]. These machines have been increasingly used in both naval and domestic applications as an alternative to conventional radial flux PM machines. Axial flux machines have numerous advantages. These machines can be stacked axially allowing for a simple construction for a range of ratings. The tape wound stator core can easily be manufactured. The airgap windings of the non-slotted axial flux machines require no slotted punchings and allows for winding shape of any kind. Improved torque/power density as well as reduced audible noise are unique features of these machines when compared with radial flux machines. There is no cogging torque due to stator or rotor teeth with airgap type stator windings for the non-slotted axial flux machines and a relatively small cogging torque for the slotted axial flux machines. In addition, ripple torque is quite small compared to the radial flux PM machines. The coils can be designed for sinusoidal MMF and smooth torque with relatively quiet operation can be achieved. The MMF harmonics can be further reduced by properly wrapping the airgap windings around the stator for the non-slotted topologies. Finally, cooling of the axial flux machines in non-slotted topologies is

relatively easy since copper windings are exposed on the surface of the stator disc.

This paper develops the principles, analysis and calculation methods of the slotted and non-slotted radial and axial flux permanent magnet motors for submersible shipboard applications. Specifically, these machines were evaluated from the perspective of noise, vibration, power density, efficiency, loss, and torque quality including torque ripple and cogging torque. Care was taken to compare the results of various surface mounted permanent magnet motor topologies. The traditional radial flux surface mounted PM machine was chosen as the benchmark comparison in this study.

2. Compared Motor Types and Motor Models

Six different 200HP 1200rpm radial and axial flux type permanent magnet machines were analyzed in a recent study [1]. Two radial flux machines, namely non-slotted radial flux surface mounted PM machine (RFSM-NS) and slotted radial flux surface mounted PM machine (RFSM-S), were investigated. The rest of the machine types were axial flux surface mounted non-slotted and slotted one-stator-two-rotor (TORUS) and two-stator-one-rotor (AFIR) type PM machines. In general, axial flux disc motors have N stators and N+1 rotors (N≥1) for external rotor & internal stator axial flux disc motor (TORUS) types and N+1 stators and N rotors (N≥1) for internal rotor & external stator axial flux disc motor (AFIR) types. The topologies used in the study are illustrated in Figure 1.

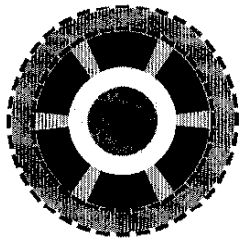

a) Radial flux surface mounted non-slotted PM motor (RFSM-NS)

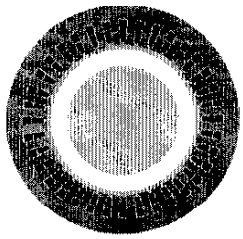

b) Radial flux surface mounted slotted PM motor (RFSM-S)

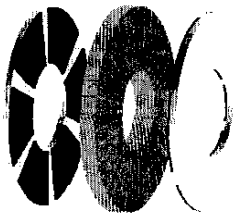

c) Axial flux external rotor & non-slotted stator motor (TORUS-NS)

d) Axial flux external rotor & slotted stator motor (TORUS-S)

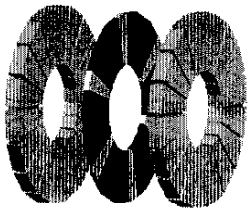

e) Axial flux internal rotor &non-slotted stator PM motor (AFIR-NS)

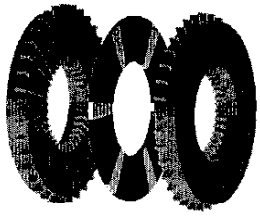

f) Axial flux internal rotor & slotted stator PM motor (AFIR-S)

Fig 1. Radial and axial flux PM motor models

3. An Approach to Motor Sizing and Performance for Comparison of Motor Types

In general, comparison of different machine types is a challenging task. S. Huang et al [5] have developed a general sizing and torque/power density equations and established a systematic method to compare the capabilities of machines with different topologies. In this section, a concept is first introduced in order to compare the torque density on the basis of the total occupied volume instead of air-gap volume. Special factors are presented to account for the effects of current and back-EMF waveforms. Finally the comparison methods are dedicated to the radial flux, the axial flux and the transverse flux machines respectively [5-7].

The general sizing equations have the following forms for both radial and axial flux machines:
For the radial flux machines [5]

$$P_R = \frac{1}{1+K_\phi}\frac{m}{m_1}\frac{\pi}{2}K_e K_i K_p \eta B_g A \frac{f}{p}\lambda_o^2 D_o^2 L_e$$

$$= \frac{1}{1+K_\phi}\frac{m}{m_1}\frac{\pi}{2}K_e K_i K_p K_l \eta B_g A \frac{f}{p} D_g^3 \qquad (1)$$

and for the axial flux machines the sizing equation can be written in the following form [6]

$$P_R = \frac{1}{1+K_\phi}\frac{m}{m_1}\frac{\pi}{2}K_e K_i K_p K_L \eta B_g A \frac{f}{p}(1-\lambda^2)\frac{1+\lambda}{2} D_o^2 L_e \qquad (2)$$

where

- P_R — rated output power of the machine,
- m — number of phases of the machine,
- m_1 — number of phases of each stator,
- K_e — EMF factor which incorporates the winding distribution factor K_w and the ratio between the area spanned by the (salient) poles and the total airgap area,
- K_i — current waveform factor,
- K_p — electrical power waveform factor,

η — machine efficiency,
B_g — airgap flux density,
A — total electrical loading,
f — converter frequency,
p — machine pole pairs,
L_e — effective stack length of the machine,
D_o, D_g, D_i — machine diameters at outer surface, air-gap surface and inner surface,
$K_\phi = A_r / A_s$ — ratio of electrical loading on rotor and stator (K_ϕ=0 for no rotor winding),
$K_l = L_e / D_g$ — aspect ratio coefficient for radial flux machines,
$K_L = D_o / L_e$ — aspect ratio coefficient for axial flux machines,
$\lambda_o = D_g / D_o$ — ratio of the diameter for radial flux machines,
$\lambda = D_i / D_o$ — ratio of the diameter for axial flux machines.

The machine torque density and power density for the total volume can be defined as

$$T_{den.} = \frac{T_R}{\frac{\pi}{4} D_{tot}^2 L_{tot}} = \frac{P_R}{\omega_m \frac{\pi}{4} D_{tot}^2 L_{tot}} \quad (3)$$

$$P_{den.} = \frac{P_R}{\frac{\pi}{4} D_{tot}^2 L_{tot}} \quad (4)$$

where T_R is the rated torque of the machine, D_{tot} is the total outer diameter of the machine including the stack outer diameter and the protrusion of the end winding from the iron stack in the radial direction, L_{tot} is the total length of the machine including the stack length and the protrusion of the end winding from the iron stack in the axial direction, ω_m is the rotor angular speed. In this case the density ratio is defined as

$$\text{Density ratio} = \frac{T_{den.}}{T_{den.-RFSM}} = \frac{P_{den.}}{P_{den.-RFSM}} \quad (5)$$

where $T_{den.-RFSM}$ and $P_{den.-RFSM}$ are the torque density and power density of RFSM machine respectively. The conventional PM machine (RFSM) is used as the benchmark for comparison of machine types.

Also, the utilization factor is expressed as

$$C_w = \frac{P_R(kW) \cdot \eta}{W_{eight}(Kg)} \quad (6)$$

where W_{eight} is the weight of the machines.

To consider the temperature rise, the heat dissipation factor is also given for both radial and axial flux machines

$$Heat\_diss = \begin{cases} \dfrac{Copper\_loss + Iron\_loss}{\pi D_o L_{tot}} & \text{RFSM} \\ \dfrac{Copper\_loss + Iron\_loss}{\pi(D_o + D_i)L_{stator} + 2(D_o^2 - D_i^2)\pi/4} & \text{TORUS (7)} \\ \dfrac{Copper\_loss + Iron\_loss}{2\pi(D_o + D_i)L_{stator} + 4(D_o^2 - D_i^2)\pi/4} & \text{AFIR} \end{cases}$$

4. A Direct Approach to Ripple Torque Level Evaluation

Pulsation torque gains importance for low noise and smooth torque applications for both radial and axial flux surface mounted PM machines. It consists of two torque components: cogging torque and ripple torque. The cogging torque arises from the variation of the airgap permeance or reluctance of the stator teeth and slots above the magnets as the rotor rotates, while the ripple torque is mainly due to fluctuations of the field distribution and the armature MMF, which depends on the motor structure and the armature current waveform. When supplied with a sinusoidal armature current, the surface mounted PM machine with a sinusoidal back EMF is ideally capable of producing a constant torque with zero ripple torque. From a machine design standpoint, a sinusoidal back EMF requires a sinusoidal distribution of magnet flux and windings. Due to limits in magnetic field and available slots for a winding distribution, harmonics in the back EMF and thus associoated pulsation torque are unavoidable. For applications requiring low pulsation torque, a practical solution in machine design seems to be airgap windings to practically eliminate the cogging torque, obtain better the sinusoidal winding distribution and decrease the ripple torque.

The torque-ripple factor (TRF) can be defined as the ratio of peak-to-peak ripple torque to average torque, which has the following form [8-9]

$$\text{TRF} = \frac{T_{pp}}{T_0} \quad (8)$$

where T_0 is the average torque and T_{pp} is peak-to-peak ripple torque which is given as

$$T_{pp} = 2\sqrt{T_6^2 + T_{12}^2 + T_{18}^2 + \ldots} \quad (9)$$

where T_{6n} are the harmonic torques. For the sinusoidal armature current case, the torque-ripple factor expression becomes [1]

$$TRF=2\frac{\sqrt{(E_7-E_5)^2+(E_{13}-E_{11})^2+(E_{19}-E_{17})^2+(E_{25}-E_{23})^2+\ldots}}{E_1}$$

$$=2\frac{\sqrt{(K_{h7}-K_{h5})^2+(K_{h13}-K_{h11})^2+(K_{h19}-K_{h17})^2+(K_{h25}-K_{h23})^2+\ldots}}{K_{h1}} \quad (10)$$

where

$$\frac{E_n}{E_1} = \frac{K_{wn}\cdot K_{sn}\cdot K_{fn}\cdot K_{osn}}{K_{w1}\cdot K_{s1}\cdot K_{f1}\cdot K_{os1}} = \frac{K_{hn}}{K_{h1}},$$

and $K_{hn}=K_{wn}\,K_{sn}\,K_{fn}\,K_{osn}$ is n^{th} harmonic factor, K_{wn} is the n^{th} harmonic winding factor, K_{fn} is the n^{th} harmonic form factor, K_{sn} is the n^{th} harmonic rotor skew factor and K_{osn} is the n^{th} harmonic open slot factor.

5. Minimization of Ripple Torque for Slotless TORUS Machine

For sinusoidal armature current case, it is possible to reduce the ripple torque to a minimum level by optimizing the PM shape and PM rotor skew angle since the ripple torque is proportional to the high-order harmonic component of EMF. This principle was used in the optimization of the TORUS-NS machine shown in Figure 1c. Analysis and calculation of torque ripple factor TRF and per unit average torque component vs. pole arc ratio $\alpha_i = w_{pm} / \tau_p$ and rotor PM pole skew angle θ_{skew} are shown from Figure 2 to 4. As can be seen from Figure 2, the TRF is minimum at a PM pole arc ratio of 0.81 as the electrical skew angle is 32.4 degrees.

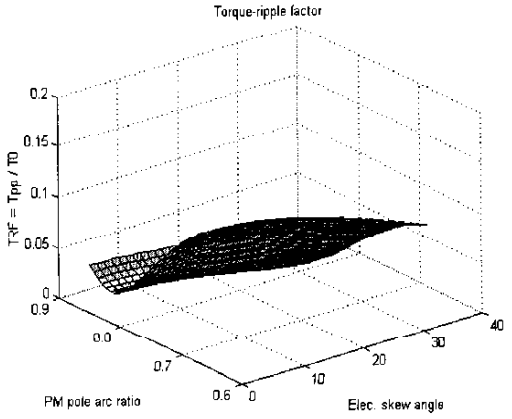

Fig 2. TRF vs. PM pole arc ratio α_i and rotor skew θ_{skew}

Figure 3 shows the average torque component as a function of PM pole arc ratio and electrical skew angle. It can be observed from the plot that average torque is quite high around the pole arc ratio of 0.81.

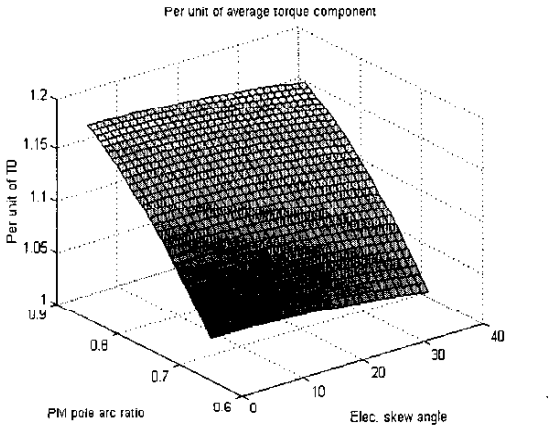

Fig 3. Average torque component [pu] vs. α_i and θ_{skew}

In addition, Figure 4 illustrates the 6th and 12th harmonic torque components as a function of pole arc ratio, α_i, and electrical skew angle, θ_{skew}. These plots show that the harmonic ripple torque curves are at a minimum near the pole arc ratio of 0.8 and electrical skew angle of 30 degrees. The same TRF plots are shown in 2D view in Figures 5 and 6 as well. Figure 5 shows the TRF as a function of the magnet pole arc ratio and the 6th and 12th harmonic torques in per unit. It can be observed from the plot that the TRF is minimum at a pole arc ratio of 0.81. Figure 6 illustrates the TRF, average torque and the amplitudes of different harmonic torques as a function of the electrical skew angle.

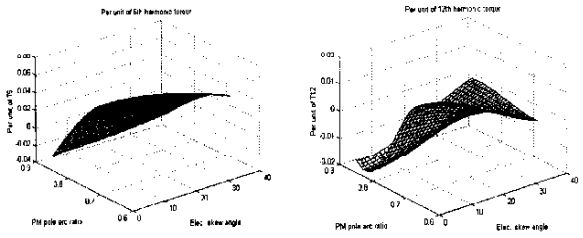

Fig 4. 6th and 12th harmonic torque component in per unit vs. α_i and θ_{skew}

Figure 7 shows the total torque, ripple torque and harmonic torques of a 200HP 1200rpm TORUS-NS machine for the optimum pole arc ratio and skewed rotor magnet case. It can be determined from the plot that the ripple torque of the non-slotted TORUS machine is very low. The peak-to-peak 6th and 12th harmonic torques have also negligible values compared to the rated torque of the machine.

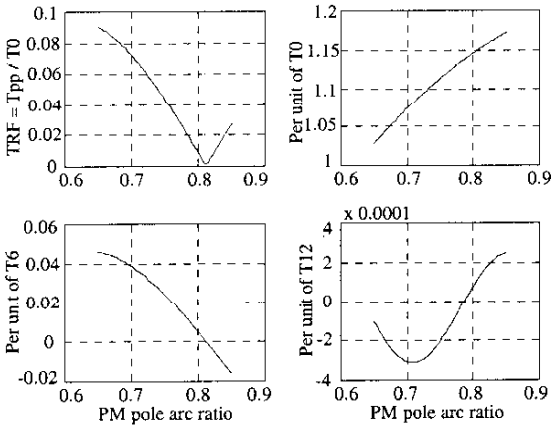

Fig 5. Per unit harmonic torque vs. PM pole arc ratio

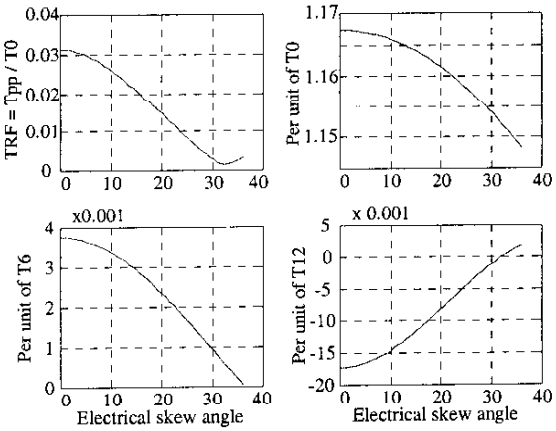

Fig 6. Per unit harmonic torque vs. electrical skew angle

Figure 8 shows the harmonic spectrum of the ripple torque in pu. As can be seen from the figure, the harmonic torques are multiples of 6 and the amplitudes are extremely low compared to the first harmonic.

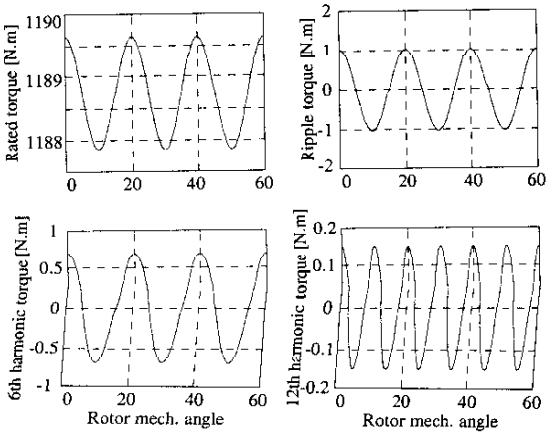

Fig 7. Torque vs. rotor position over one pole pair

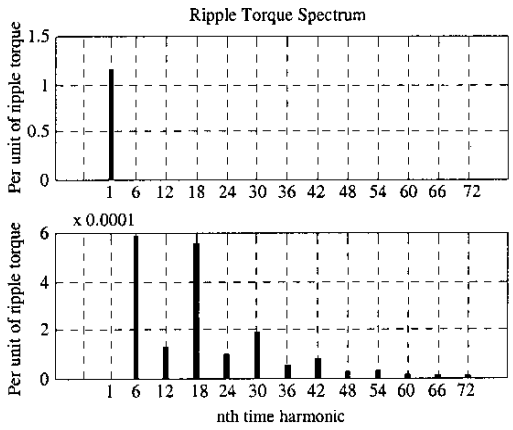

Fig 8. Spectrum of the ripple torque in [pu]

6. Vibration Displacement Due to Exciting Forces

According to the mechanical impedance method theory, the vibration displacement mode number and frequency can be derived as [1]

$$Y_{r/f_r} = \begin{cases} \dfrac{P_{eq-r/f_r}}{(k_{r-core}+k_{r-frame})-\omega_r^2(m_{r-core}+m_{r-frame})} & \text{For radial flux topologies} \\ \dfrac{P_{eq-r/f_r}}{k_{r-core-rotor}-\omega_r^2 m_{r-core-rotor}} & \text{For TORUS topologies} \\ \dfrac{P_{eq-r/f_r}}{k_{r-core-stator}-\omega_r^2 m_{r-core-stator}} & \text{For AFIR topologies} \end{cases} \quad (11)$$

where P_{eq-r/f_r} is the equivalent exciting force in the airgap surface of the mode number and frequency concerned, $\omega_r = 2\pi f_r$ is the radian frequency of the exciting force waves, $k_{r-core-rotor}$ is the equivalent spring stiffness of the external rotor core including rotor PM for the TORUS topologies, $k_{r-core-stator}$ is the equivalent spring stiffness of the external stator core including stator windings and teeth for the AFIR topologies.

The equivalent exciting force in the airgap surface for the mode number and frequency is

$$P_{eq-r/f_r} = S_g \, P_{peak-r/f_r} \quad (12)$$

where P_{peak-r/f_r} is the amplitude of the exciting force waves for the mode number and frequency concerned.

The airgap surface area is

$$S_g = \begin{cases} \pi D_g L_{eff} & \text{for radial flux topology} \\ \frac{\pi}{4}(D_0^2 - D_i^2) & \text{for axial flux topology} \end{cases} \quad (13)$$

According to Maxwell's equations, the magnitude of the exciting force is proportional to the square of the normal component of the air gap flux density.

$$p_{ef}(\theta,t) = \left\{ \frac{b^2(\theta,t)}{2\mu_0} \right. \quad (14)$$

where $p_{ef}(\theta,t)$ is the exciting force wave (force per unit area [N/m^2]), $b(\theta,t)$ is the airgap flux density waves, $\mu_0 = 4\pi\times10^{-7}$ [H/m] is the permeability of free space, θ is the space coordinate in radians. It should be noted that the exciting force is in the radial direction for radial flux machines and in the axial direction for axial flux machines in this equation. Also, the amplitude of the vibrating velocity of machine is given by

$$V_{pk-r} = \omega_r Y_{pk-r} \quad (15)$$

where Y_{pk-r} is the amplitude of the particle vibratory displacement.

7. Resultant Sound Power Level

The surface vibration of machines due to the exciting force waves may be regarded as a series of rotating sinusoidal waves of displacement. Yang's (1975) equation of the sound power for the cylindrical sound wave model is [10].

$$W_{Cylin-r} = 2\rho C\pi^2 f_r^2 Y_{pk-r}^2 S_{Cylin} I_{re-r} \quad (16)$$

where ρ is the density of the medium (for air ρ=1.186 kg/m^3), f_r is the frequency of the sound wave, C is the traveling speed of sound in the medium (for air, C =344 m/s), S_{Cylin} is the surface vibration area for the radial flux cylindrical machine which is perpendicular to the direction of travel of sound and I_{re-r} is the relative sound intensity coefficient.

The sound power for the plane sound wave model can be expressed as [1]

$$W_{plane-r} = 2\rho C\pi^2 f_r^2 Y_{pk-r}^2 S_{plane} I_{re-r} \quad (17)$$

where S_{Plane} is the surface vibration area for the axial flux disc machines and this area is perpendicular to the direction of the travel of sound. Finally the resultant sound power level is defined as

$$L_{Wt} = \sum_{i=1}^{n} L_{Wi} = 10\log\left[\sum_{i=1}^{n}\frac{W_i}{W_0}\right] = 10\log\left[\sum_{i=1}^{n} 10^{0.1L_{Wi}}\right] \text{[dB]} \quad (18)$$

where $L_{Wi} = 10\log(W_i/W_0)$ [dB], W_i is the sound power [W], W_O=10^{-12} [W] is the reference value of the sound power.

8. Comparison and Conclusions

Sizing analysis of 200 HP auxiliary motors was accomplished and the summary of the analysis is given in Figures 9a through 9e. It can be concluded that TORUS slotted and non-slotted topologies have higher power or torque density ratio compared to other RFSM and AFIR topologies. The efficiencies of all the topologies are quite high and very close to each other. Also, slotted and non-slotted AFIR topologies have the lowest weights among the others. Particularly, AFIR-S topology has the lowest weight and highest utilization factor. Moreover, in general, axial flux non-slotted topologies are always better than axial flux slotted topologies in terms of torque density, efficiency and heat dissipation.

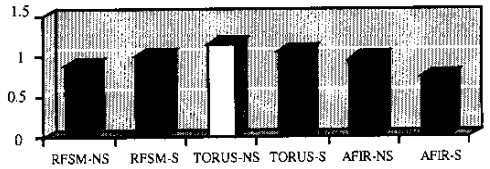

Fig 9a. Power/torque density comparison [ratio]

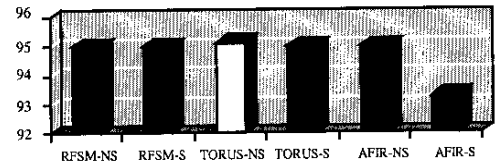

Fig 9b. Efficiency comparison [%]

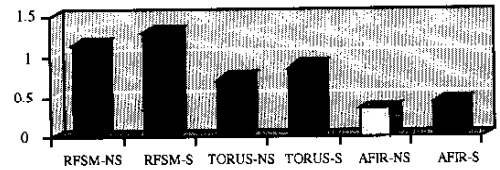

Fig 9c. Heat dissipation comparison [W/cm^2]

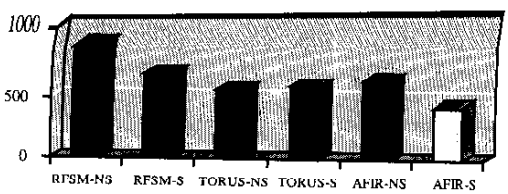

Fig 9d. Weight comparison [lb]

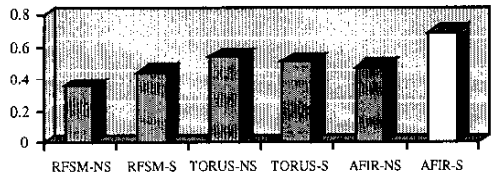

Fig 9e. Utilization factor comparison [kW/Kg]

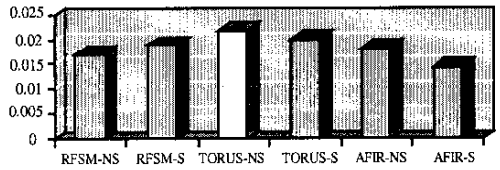

Fig 9f. Torque density comparison [Nm/cm^3]

A comparison of the topologies in terms of cogging torque and ripple torque was also realized for slotted and non-slotted machines using 2D and 3D Finite Element Analysis. The models were first operated at no load for different rotor positions and cogging torque variations were investigated. Pulsating torque values were then determined for the loaded case using the same approach. Since the ripple torque is defined as the difference between the pulsating torque and the cogging torque, the ripple torque components of the machines can then easily be obtained. The cogging torque and ripple torque results are shown in Figures 10 and 11 without and with skewed rotor magnets. It can be concluded from this analysis that non-slotted topologies have negligible cogging torque as can be seen in Figure 10. The cogging torque is the highest for the conventional PM machine (RFSM-S) and can be reduced more by skewing either rotor magnets or stator slots. Besides, in general, non-slotted machines have lower ripple torque than slotted machines for unskewed magnet case as can be observed from Figure 11. The non-slotted version of the TORUS machine has the lowest ripple torque compared to the other topologies.

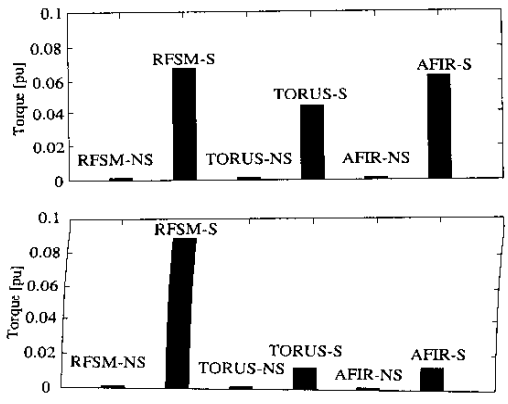

Fig 10.Cogging torque without and with skewed rotor PMs [pu]

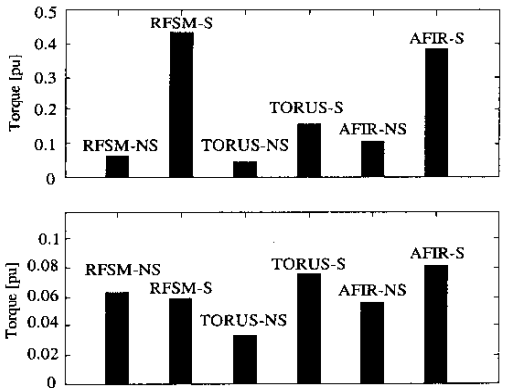

Fig 11. Ripple torque without and with skewed rotor PMs [pu]

The resultant sound power levels, maximum vibration velocities and maximum vibration displacement of main vibration source values are shown in Figure 12a through 12f. It should be noted that both high and low frequency ranges of vibration exist in any machine. The high frequency range of vibration is the main source of acoustics compared to low frequency range of vibration and causes the main acoustic noise that is in the range of human ear. However, the low frequency range of vibration is the main vibration source compared to high frequency vibration. Skewing reduces the high frequency noise. As the thickness of the frame and core increases, the equivalent spring stiffness increases, which results in reduced low frequency vibration.

Non Skewed Rotor PM – Full-load Case:

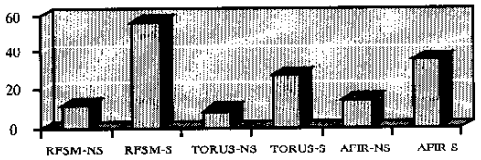

Fig 12a. Resultant sound power level (L_{wr}) [dB]

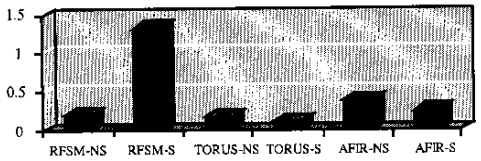

Fig 12b. Maximum vibration velocity of main vibration source (*Vel_max*) [rms-mm/s]

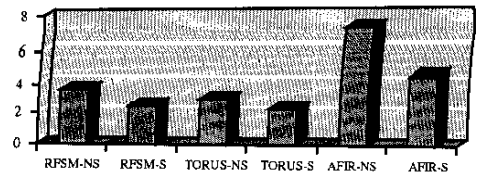

Fig 12c. Maximum vibration displacement of main vibration source (*Y_max*) [peak-mm/s]

Skewed Rotor PM – Full-load Case:

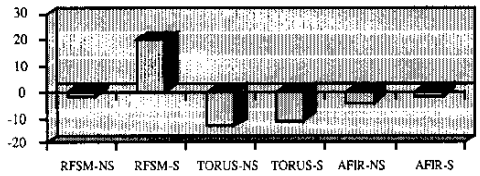

Fig 12d. Resultant sound power level (L_{wr}) [dB]

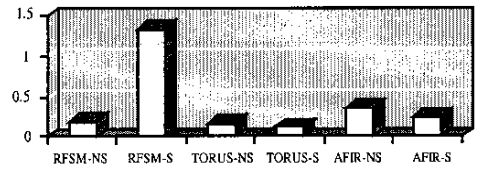

Fig 12e. Maximum vibration velocity of main vibration source (*Vel_max*) [rms-mm/s]

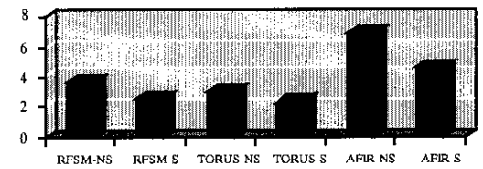

Fig 12f. Maximum vibration displacement of main vibration source (*Y_max*) [peak-mm/s]

From this information and data gathered, it can be concluded that in general non-slotted topologies have lower sound power levels than slotted topologies. Especially, TORUS-NS topology has the lowest sound power level. In addition, skewed rotor magnets reduce the noise level and high frequency vibration. TORUS-S machine has the highest spring stiffness and lowest vibration displacement compared to other topologies. The non-slotted version of the TORUS machine has the highest torque/power density, highest efficiency, lowest noise level and lower vibration displacement. Finally, the conventional radial flux slotted PM machine has the highest noise and vibration level compared to the other topologies.

Acknowledgements

The authors are grateful to the Naval Surface Warfare Center for their financial support (Grant Number: N00014-98-1-0807).

References

[1] T. A. Lipo, S Huang and M. Aydin, "Performance Assessment of Axial Flux Permanent Magnet Motors for Low Noise Applications", Final Report to ONR, Oct 2000.

[2] P. Campbell, "Principles of a Permanent-Magnet Axial-Field DC Machine", Proc. IEE, Vol. 121, No. 12, Dec. 1974, pp. 1489-1494.

[3] E. Spooner and B. J. Chalmers, "TORUS, A Toroidal-Stator, Permanent Magnet Machine for Small Scale Power Generation", International Conference on Electrical Machines 1990, MIT, Cambridge, pp. 1053-1058.

[4] C. C. Jensen, F. Profumo and T. A. Lipo, "A Low Loss Permanent Magnet Brushless DC Motor Utilizing Tape Wound Amorphous Iron", IEEE Transactions on Industry Applications, Vol. 28, No. 3, May/June 1992, pp. 646-651.

[5] S. Huang, J. Luo, F. Leonardi, and T. A. Lipo, "A General Approach to Sizing and Power Density Equations for Comparison of Electrical Mac-hines," IEEE Transactions on Industry Applica-tions, Vol.34, No.1, January/February 1998, pp. 92-97.

[6] S. Huang, J. Luo, F. Leonardi and T. A. Lipo, "A Comparison of Power Density for Axial Flux Machines Based on the General Purpose Sizing Equation", IEEE Transactions on Energy Conver-sion, Vol.14, No.2 June 1999, pp. 185-192.

[7] S. Huang, J. Luo and T. A. Lipo, "Analysis and Evaluation of the Transverse Flux Circumferential Current Machine", Conference Record of the 1997 IEEE Industry Applications Society, 32nd IAS Annual Meeting, pp. 378-384.

[8] H. Le-Huy, R. Perret and R. Feuillet, "Minimization of Torque Ripple in Brushless DC Motor Drives", IEEE Transactions on Industry Applications, Vol.22, No.4, July/August 1986, pp. 748-755.

[9] T. Sebastian and V. Gangla, "Analysis of Induced EMF Waveforms and Torque Rripple in a Brushless Permanent Magnet Machine", IEEE Trans. on Industry Applications, Vol.32, No.1, January/February 1996, pp. 195 200.

[10] S.J. Yang, "Low-noise Electrical Motors", Clarendon Press, Oxford, 1981.